

# Escaping Plato’s Cave: Robust Conceptual Reasoning through Interpretable 3D Neural Object Volumes

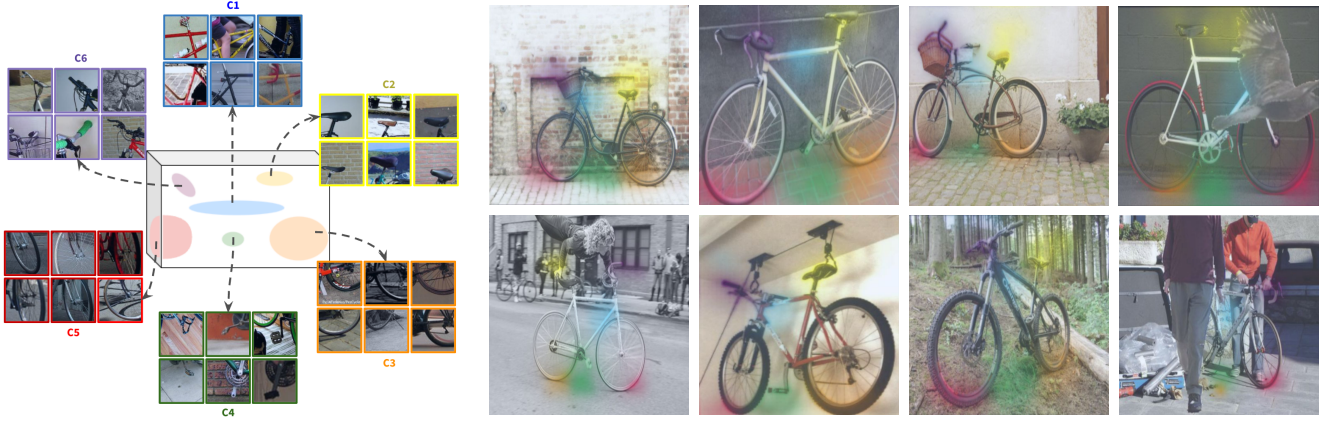
Nhi Pham<sup>1</sup> Bernt Schiele<sup>1</sup> Adam Kortylewski<sup>\*1,2</sup> Jonas Fischer<sup>\*1</sup>

<sup>1</sup>Max Planck Institute for Informatics, Saarland Informatics Campus, Germany

<sup>2</sup>University of Freiburg, Germany

\*Equal senior advisorship

{nhiphamp, schiele, akortyle, jonas.fischer}@mpi-inf.mpg.de



(a) Concept-aware volume for class Bicycle.

(b) Attributions of concepts in images of bicycles in different poses show spatial consistency.

Figure 1. We introduce **Concept Aware Volumes for Explanations (CAVE)**. **(a)** We learn 3D object volumes, here cuboids, with concept representations. Each concept captures distinct local features of objects. **(b)** At inference, these concepts are matched with 2D image features, achieving robust and interpretable image classification. We further highlight the 3D consistency of these concepts in Fig. 5.

## Abstract

With the rise of neural networks, especially in high-stakes applications, these networks need two properties (i) robustness and (ii) interpretability to ensure their safety. Recent advances in classifiers with 3D volumetric object representations have demonstrated greatly enhanced robustness in out-of-distribution data. However, these 3D-aware classifiers have not been studied from the perspective of interpretability. We introduce CAVE – Concept Aware Volumes for Explanations – a new direction that unifies interpretability and robustness in image classification. We design an inherently-interpretable and robust classifier by extending existing 3D-aware classifiers with concepts extracted from their volumetric representations for classification. In an array of quantitative metrics for interpretability, we compare against different concept-based approaches across the explainable AI literature and show that CAVE discovers well-

grounded concepts that are used consistently across images, while achieving superior robustness.

## 1. Introduction

Deep neural networks (DNNs) have achieved impressive performance in diverse domains ranging from healthcare to autonomous driving. However, their decision-making processes remain largely opaque. They have already been shown to depend on spurious correlations [28], raising concerns about their reliability. In high-stake and critical applications such as healthcare or judicial justice, ensuring *interpretability and robustness* is not just desirable – it is essential for safety and trustworthiness.

To overcome such issues and make networks more transparent and interpretable, various approaches have been proposed in the scope of explainable AI (XAI). Notably, post-hoc methods generate concept-based explanations for pre-

trained networks [2, 10, 11, 18, 36], providing insights into their decision-making process without altering the underlying architecture. However, such methods can only approximate the model’s computations, and thus do not provide a faithful explanation. In contrast, another line of research [1, 5, 7, 25, 26, 29] enforces interpretability directly during training, making aspects of the model inherently interpretable and ensuring that the explanations remain faithful to its decision-making process. Although these approaches show promising results with respect to interpretability, they are often not designed with robustness in mind.

DNNs deployed in real-world scenarios typically encounter distribution shifts over time, out-of-distribution (OOD) events such as occlusions, or adverse weather conditions in the case of autonomous driving. In consequence, not only the model itself, but also any explanations extracted from a representation in the model are unreliable. In a scenario where about 40% of a car is occluded, other methods usually fail to accurately recognize the object or produce meaningful explanations (cf. Fig. 11). In an orthogonal line of research, it has been shown that incorporating 3D compositional object representations into the training pipeline significantly improves OOD robustness [20], yet these classifiers remain inherently opaque, leaving a critical gap in understanding their decision making.

These current limitations of image classification are reflected in the allegory of the cave by Plato, which gives a philosophical argument for the issues arising with observing a 3D world by 2D images alone. In the story, prisoners have been chained to a cave wall and have never seen anything else but the (2D) shadows of objects cast on the opposing wall. The prisoners consider the 2D world of shadows their reality and, when freed from the prison, would not accept the reality, which is three-dimensional, color- and light-ful, as truth. In analogy, a model (the prisoner) that has only seen 2D images, which are projections of our world (the shadows), is not able to reason beyond these projections to OOD data (color and light outside the cave), and is not able to provide spatially consistent and meaningful conceptual understanding (true 3D world). Here, we *escape* the dilemma of Plato’s cave by learning *concept-aware neural object volumes*, which allow for *robust and inherently interpretable* image classification.

In particular, we introduce CAVE (Concept Aware Volumes for Explanations), a model that leverages learned 3D-aware neural object volumes for each class, which are then projected into images for classification. In a nutshell, each class is represented by a cuboid with features – represented as high-dimensional vectors – on its surface. These features are learned to align with the latent features of a (2D) backbone, orienting the cuboid through the given pose during training. We then summarise these features on the cuboid to form higher-level concepts which can be annotated via

an attribution approach that we specifically develop for this architecture (cf. Fig. 1). By design, this model is inherently interpretable, as we use the feature representations of the higher-level concepts for classification, similar to the classification layer in a concept bottleneck model [21, 29]. In analogy to Plato’s cave, we learn the object (with its conceptual features) that was used to cast the shadow rather than learning the features of the shadow, thus escaping the cave.

We evaluate CAVE in comparison to a wide array of existing XAI methods, including post-hoc and inherently interpretable approaches ranging from concept extraction, over inherent concept learning to prototype learning. For evaluation, we consider OOD datasets to assess *robustness* and consider a variety of different benchmark metrics for *interpretability*, where CAVE shows to offer a unique combination of robustness and interpretability, outperforming existing works by a margin.

In summary, our **contributions** include:

- (i) the CAVE model for robust and interpretable image classification through neural object volumes,
- (ii) a formulation of concept attribution for image classifiers with neural volumes,
- (iii) a novel metric for 3D consistency of concepts, and
- (iv) a comprehensive evaluation comparing CAVE to different XAI approaches and on a variety of quantitative benchmark metrics.

## 2. Related Work

**3D Information for 2D Understanding.** In different fields of computer vision, 3D information has been shown invaluable for effective 2D feature representations, which are essential for down-stream tasks including segmentation or depth estimation [15, 19, 41]. While powerful, these approaches usually require rich data of images from different camera-poses. Recently, NOVUM [20] pioneered using 3D information effectively for robust classification, by considering 3D pose information to fit neural object volumes to an image. This line of work forms the basis of our approach.

**Concept-based Explanations.** To make model decisions transparent, one focus of XAI has been the discovery of *concept representations* in models. For post-hoc concept discovery, CRAFT [12, 36] and ICE [42] use matrix factorization to extract concept bases from recorded activations, while MCD [37] uses a sparse subspace clustering approach to recover concept subspaces in the activation space. PCX [9] learns concepts on relevances of features instead of activations. ExplaiNN [13] uses pattern mining to identify neuron combinations that encode concepts. Recently, inherently interpretable concept-based methods such as the concept bottleneck model (CBM) [21] have been proposed, where a concept layer is inserted as the penultimate layer, with each neuron encoding a specific, human-

understandable concept. Closely related are sparse autoencoders [24], which often serve as basis for CBM models. While most CBM approaches require data with concept annotation, label-free CBMs instead use an LLM to generate class-specific concepts, thus not requiring such heavy annotation [29]. Almost directly related to concept-based explanations is *prototype learning*, with ProtoPNet [7] as one of the earliest approaches discovering prototypical image features whose presence are then used to classify, resembling a “this looks like that” explanation. The follow-up work includes TesNet [39] and PIP-Net [26], which improve various aspects of the training and prediction pipeline for prototype networks. For a comprehensive overview, we refer to Li et al. [22]. For a comprehensive evaluation, we evaluate our method against CRAFT, MCD, ICE, PCX, LF-CBM, ProtoPNet, TesNet, and PIP-Net.

**Attributing Relevant Features.** For an understanding of which visual features a concept responds to, up-sampled feature maps of, e.g., prototypes in ProtoPNet, or classical attribution methods [4, 30, 32, 33, 35] are frequently used. None of these attributions is tailored for a neural object volume-based classifier. Therefore, in this paper, we adapt and extend LRP [4, 30] to be able to attribute concepts to input features.

### 3. CAVE: A 3D-Aware Inherently Interpretable Classifier

Our goal is to build an image classifier with two key properties: (1) robust classification in OOD settings, and (2) inherently interpretable model predictions. Specific solutions for each of these individual properties exist; however, combining them is far from trivial. Here, we use learned neural object volumes [20] as the basis for our approach. In brief, each object class is represented by a 3D cuboid mesh with surface features represented by high-dimensional vectors. During training, leveraging available 3D pose information, the cuboid is projected into the given 2D image and the features from the surface are learned to align with the corresponding features of the 2D image extracted through a standard backbone model (e.g., a ResNet-50). At inference, an image is passed through the backbone and the resulting latent features are matched with the volume features. The class represented by the maximally aligned volume is the output. As such, the volumes are 3D-aware, robust feature representations of the given object classes, thus alleviating Plato’s dilemma of the cave. We provide a more formal recap of this approach in Sec. 3.1.

While neural object volumes are robust, their composition through thousands of feature vectors on the surface, as well as the classification process itself, are not interpretable. To overcome this limitation, we first show how to extract a sparse, representative set of interpretable concepts from

Dataset	P3D+	Occluded-P3D+			OOD-CV	P-Part
Occlusion	0	[20, 40]	[40, 60]	[60, 80]	-	0
NOVUM	0.010	0.007	0.004	0.003	0.008	0.007
CAVE (Ours)	<b>0.715</b>	<b>0.557</b>	<b>0.377</b>	<b>0.246</b>	<b>0.566</b>	<b>0.544</b>

Table 1. **Average confidence gap ( $\uparrow$ , %) for correct predictions**, measured between the top two softmax scores across all classes in Pascal3D+ (P3D+) [40], Occluded Pascal3D+ [38] (occlusion levels in %), OOD-CV [43] (5 nuisance factors on pose, shape, context, texture, weather), and same classes in Pascal-Part (P-Part) [8].

the volume features (cf. Fig. 1a). We then modify the volume to be covered by representative feature vectors of these concepts and show how to classify based on these modified volumes, making the classification inherently interpretable in Sec. 3.2. We give an overview of this approach in Fig. 2.

The learned concepts need to be matched to features in the input image, for which we are proposing to define an attribution method, properly reflecting the volume-based classification process. Therefore, in Sec. 3.3, we show how to define conservation rules to compute layer-wise relevance propagation (LRP) for this purpose.

### 3.1. Classification Through Neural Object Volumes

In a general supervised setting, an image classifier consists of a feature extractor  $f(\cdot)$  and a classification layer. Given a test input image  $x$ , the feature extractor produces a feature map  $F_x = f(x) \in \mathbb{R}^{H \times W \times C}$ , where  $C$  is the number of channels, and  $H, W$  are the spatial dimensions. We use  $f_i(x)$  to indicate the feature vector for the  $i$ -th pixel in raster order, and drop  $x$  when it is clear from context.

The 3D-aware classifier NOVUM [20], introduces a feature matching  $\mathcal{M}(\cdot)$  of neural object volumes (NOVs) with the output of the feature extractor  $f(\cdot)$  for the classification. Before describing the feature matching  $\mathcal{M}$ , we first formally define NOVs. A NOV is a representation of an object of class  $y$ , and is defined as a set of  $K$  3D Gaussians. Each Gaussian  $k$  is characterised by a position in 3D space  $\mu_y^{(k)} \in \mathbb{R}^3$  and a fixed unit variance and additionally is associated with a feature vector  $g_y^{(k)} \in \mathbb{R}^C$ . NOVUM fixes the Gaussian positions to form a regular grid on the surface of a cuboid. We define the matrix of Gaussian features for the object class  $y$  as  $\mathcal{G}_y \in \mathbb{R}^{K \times C}$ , which will be later used to match with the feature map  $F_x$  from the backbone model. Extending this notation, the complete matrix of Gaussian features across all  $M$  object classes can be represented as  $\mathcal{G} = [\mathcal{G}_1; \mathcal{G}_2; \dots; \mathcal{G}_M] \in \mathbb{R}^{MK \times C}$ .

The feature matching  $\mathcal{M}$ , as in [20], aligns each feature  $f_i \in F_x$  from the backbone feature map with the most similar Gaussian feature across  $\mathcal{G}$  from the 3D object representation. The logit for class  $y$  is computed by summing over all spatial locations where feature  $f_i$  is matched to a Gaussian

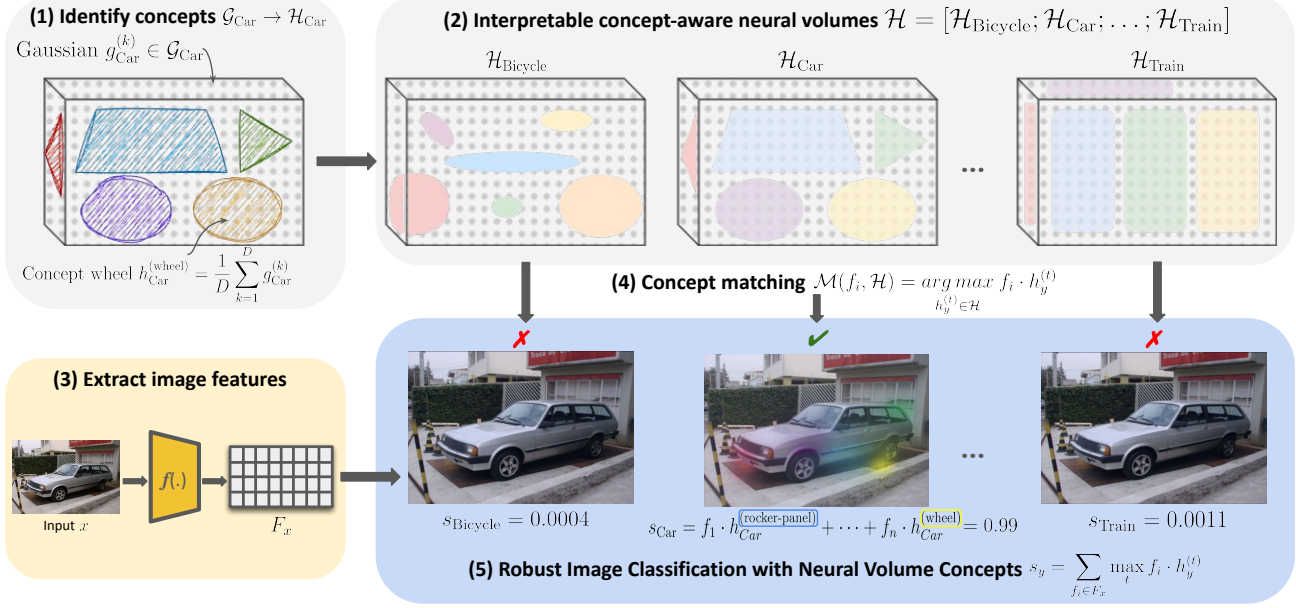


Figure 2. **Overview pipeline of Concept Aware Volumes for Explanations (CAVE)**, a framework that allows for robust conceptual reasoning and classification through interpretable 3D-aware neural object volumes (NOVs). **(1)** Given the NOV of class Car, CAVE first extracts concepts via clustering on Gaussian features  $g_{\text{Car}}^{(k)}$  and represent the mean feature of each Gaussian cluster as a concept  $h_{\text{Car}}^{(t)}$ . Note that the clusters here are visually refined for illustrative purposes to better convey our method. For classification, CAVE combines image features  $F_x$  in **(2)** and interpretable concept-aware NOVs  $\mathcal{H}$  in **(3)** through a bag-of-word concept matching step **(4)**, where each feature  $f_i \in F_x$  is best aligned with  $\mathcal{H}$  by cosine similarity. The logit for class  $y$  is computed as the sum of cosine similarities over  $F_x$ , considering only features mapped to its cluster **(5)**.

feature of  $y$ :

$$s_y = \sum_{f_i \in F_x} \max_k f_i \cdot g_y^{(k)}.$$

The class with the highest score  $s_y$  is the predicted label. This formulation gives rise to 3D-aware classification through a bag-of-words feature matching mechanism, where image features are directly compared against 3D-aware Gaussian features. However, this classification process remains inherently opaque. The number of Gaussian features involved in the matching step in the order of tens of thousands makes it difficult to interpret which features contribute to the final decision.

### 3.2. Identifying Concepts Through NOVs

To achieve an inherently interpretable NOV-based classifier, we first extract a meaningful concept basis from each NOV and replace the latter with these concepts at inference time. Formally, for a volume  $\mathcal{G}_y \in \mathbb{R}^{K \times C}$  of class  $y$ , we formulate our class-wise concept extraction problem through the lens of dictionary learning [12, 23]

$$(W_y^*, \mathcal{H}_y^*) = \arg \min_{W_y, \mathcal{H}_y} \| \mathcal{G}_y - W_y \mathcal{H}_y^\top \|_F^2,$$

where weight matrix  $W_y^* \in \mathbb{R}^{K \times D}$  and the dictionary of  $D$  concept vectors  $\mathcal{H}_y^* = [h_y^{(1)}, \dots, h_y^{(D)}]^T \in \mathbb{R}^{D \times C}$  minimise the element-wise distance between our Gaussian features  $\mathcal{G}_y$  and  $W_y \mathcal{H}_y^T$ . In the case of hard clustering, the weight matrix  $W_y^*$  reduces to a discrete assignment matrix, where each row is a one-hot encoding that corresponds to only one concept. This allows clustering to be much more interpretable than methods with less sparse weight matrices.

There are different established approaches to obtain the decomposition  $\mathcal{G}_y \approx W_y \mathcal{H}_y^T$ , specifically K-Means, Principal Component Analysis (PCA) and Non-negative Matrix Factorisation (NMF). We aim to strategically select the concept extraction method that encourages disentangled, part-based concepts while maintaining competitive performance and faithfulness. To do so, we conduct a small ablation (cf. A. 8) and compare in terms of three key metrics: (i) *accuracy*, (ii) *sparsity*, and (iii) *feature distribution distance (FDD)*. Here, *sparsity* is measured following the approach in [12], which quantifies how sparse the weight matrix  $W_y^*$  is. *FDD* measures the divergence between the original distribution of  $\mathcal{G}_y$  and its new representation  $\mathcal{H}_y$ , thereby quantifying how *faithful* the latter preserves the former. After evaluating these three metrics, we select K-Means cluster-

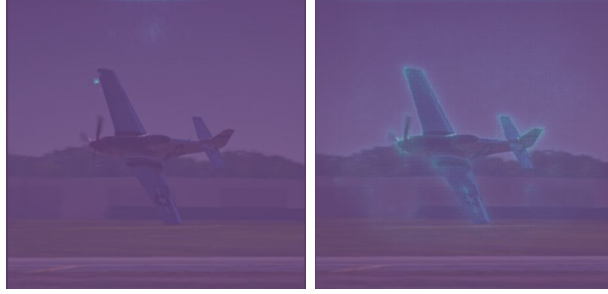


Figure 3. **Comparison between standard LRP and our volume-aware LRP.** **Left:** Standard LRP implementation from Zennit [3] attributing only individual pixels. **Right:** LRP for CAVE, which ensures proper conservation of relevance scores.

ing for concept identification in our method.

The extracted concept dictionary  $\mathcal{H}_y$  is now seen as a *sparse and interpretable* NOV to replace the original dense NOV  $\mathcal{G}_y$ . We modulate the original feature matching  $\mathcal{M}(F_x, \mathcal{G})$  in NOVUM with  $\mathcal{M}(F_x, \mathcal{H})$  that establishes correspondences between  $F_x$  and new volumetric representation  $\mathcal{H} = [\mathcal{H}_1; \mathcal{H}_2; \dots; \mathcal{H}_M] \in \mathbb{R}^{MD \times C}$ . This reformulation ensures that feature matching is performed against a compact, interpretable set of concept vectors rather than thousands of Gaussian features, all while maintaining competitive robust performance. This constitutes the first step in our CAVE framework and already improves the confidence of predictions compared to original NOVUM (see Tab. 1).

### 3.3. Attribute Concepts Through NOVs with LRP

We want to transform our extracted NOVs  $\mathcal{H}$  into human-interpretable explanations, thereby demonstrating the model’s reasoning through neural volumetric concepts. To do so, we leverage LRP, an existing attribution method that traces relevances from the model’s prediction backward to the input pixels [4, 30]. One key element of LRP is the conservation property, which means that the total relevance should remain constant throughout the network [30].

LRP is, however, only defined for standard architectures and does not yield meaningful attributions for NOV-based classifications, attributing only to a few pixels rather than correctly to whole object features (see Fig. 3 left).

In the following, we introduce LRP for NOVUM and CAVE-like architectures (cf. Fig. 4, Sec. 3.3.1). We further show how to estimate concept-wise importance scores in Sec. 3.3.2, and provide concept visualisation details in Sec. 3.3.3.

#### 3.3.1. LRP with Conservation for CAVE

(i) **Upsampling by concatenation.** The basic NOVUM contains a feature extractor which consists of a ResNet-50 backbone followed by three upsampling layers with concatenation. In this design, each upsampling layer combines

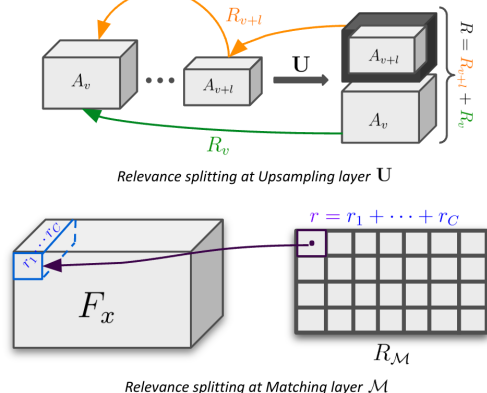


Figure 4. **Illustration of relevance propagation in CAVE.** **Top:** At an upsampling layer  $U$ , feature maps  $A_v$  and  $A_{v+l}$  from non-consecutive layers are concatenated after padding for dimensional consistency. The relevance score  $R$  is split into  $R_v$  and  $R_{v+l}$ , where  $R_{v+l}$  is masked to exclude padding contributions. **Bottom:** We ensure spatial consistency by mapping relevance  $R_M$  from the matching layer to the corresponding feature  $f_i \in F_x$ , then distributing channel-wise with NOV-weighted feature importance.

feature maps from earlier layers, preserving fine-grained details important for 3D-aware classification. Let us consider an upsampling layer  $U$ , which concatenates feature maps  $A_v \in \mathbb{R}^{H_1 \times W_1 \times C_1}$  and  $A_{v+l} \in \mathbb{R}^{H_2 \times W_2 \times C_2}$  from two non-consecutive layers.  $A_{v+l}$  is padded to  $A'_{v+l} \in \mathbb{R}^{H_1 \times H_2 \times C_2}$  to maintain dimensional consistency. Let us further denote  $R$ ,  $R_v$ , and  $R_{v+l}$  as the relevance scores at the upsampling layer and two non-consecutive layers, respectively. By conservation property, it should hold that  $R = R_v + R_{v+l}$ . We define a relevance-preserving splitting as follows:

$$R'_{v+l} = R[:, C_2, : H_1, : W_1], \quad R_{v+l} = R'_{v+l} \cdot \mathbf{1}(A_{v+l}), \\ R_v = R[C_2 : (C_1 + C_2), H_1 : 2H_1, W_1 : 2W_1],$$

where  $\mathbf{1}(\cdot)$  is the indicator function that is 1 for original non-padded elements in  $A_{v+l}$  and 0 otherwise. After three upsampling layers, we obtain our feature map  $F_x$  for 3D-aware concept matching.

(ii) **Volume concept matching.** For the concept matching  $\mathcal{M}(F_x, \mathcal{H})$  between NOVs-based concepts  $\mathcal{H}$  and image features  $F_x \in \mathbb{R}^{H \times W \times C}$ , let the output be  $s_M \in \mathbb{R}^{H \times W}$ . We further denote  $R_M \in \mathbb{R}^{H \times W}$  as the relevance for the feature matching layer, and  $R_{F_x} \in \mathbb{R}^{H \times W \times C}$  as the relevance of the feature map  $F_x$ . To ensure spatial consistency, a relevance score  $r_i \in R_M$  is first directly mapped to the corresponding feature  $f_i \in F_x$ , and then further distributed *channel-wise* (cf. Fig. 4). We thus get

$$R_{F_x}^{\text{spatial}}(i) = R_M(i) = r = \sum_{j=1}^C r_j = \sum_{j=1}^C (f_i \odot \mathcal{H}_{f_i})(j),$$

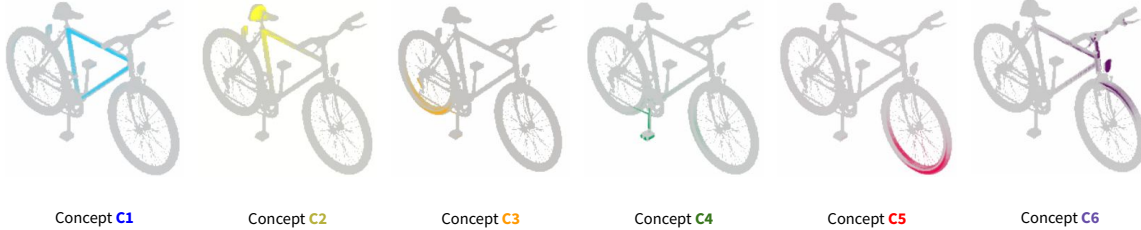


Figure 5. **3D consistency of concepts.** We highlight how consistent a concept is mapped to an object part in 3D ground-truth CAD models. Here we show 6 concepts of class Bicycle corresponding to those in Fig. 1, where each illustrates the aggregated concept relevance scores across 100 test images onto the mesh surface.

$$R_{F_x}(i, c) = R_{F_x}^{\text{spatial}}(i) \cdot \frac{(f_i \odot \mathcal{H}_{f_i})(c)}{\sum_j (f_i \odot \mathcal{H}_{f_i})(j)},$$

where  $\mathcal{H}_{f_i}$  denotes the matching NOV-based concept for  $f_i$ .

We integrate our formulation with LRP with conservation for ResNet-50 [30], which served as our feature extractor. In Fig. 3, we provide the difference between original LRP and NOV-aware LRP computations.

### 3.3.2. Concept Importance Through Volume Alignment

Our next goal is to estimate the importance of all class-wise concepts in  $\mathcal{H}_y$  using the previously-established LRP attributions. The intuition behind this is straightforward: starting from the model’s softmax output, we trace back relevance to each concept. The concept importance score is then determined using its  $x\%$  quantile (e.g., 90th percentile) across the training dataset to capture the most representative high-relevance values while being robust to outliers.

We denote the matching NOV-based concept in  $\mathcal{H}$  for the feature map  $F_x$  as  $\Delta_{F_x \rightarrow \mathcal{H}}$ . We compute the relevance for a concept  $h_y^{(t)} \in \mathcal{H}$  of class  $y$  by aggregating the relevance scores in  $R_{\mathcal{M}}$  at all spatial locations  $i$  where  $\Delta_{F_x \rightarrow \mathcal{H}}(i) = h_y^{(t)}$ . Formally, it is defined as:

$$R_{h_y^{(t)}} = \sum_{i \in H \times W} R_{\mathcal{M}} \cdot \mathbb{1}_{\Delta_{F_x \rightarrow \mathcal{H}}(i) = h_y^{(t)}}.$$

### 3.3.3. Visualising Concepts

We obtain class-wise explanations via the visualisation of NOV-based concepts  $h_y^{(t)} \in \mathcal{H}$ . Given the corresponding relevance concept score  $R_{h_y^{(t)}}$ , we re-distribute this score throughout the network as defined in Sec. 3.3.1 to obtain a relevance map at pixel space. We visualise all pixel locations that positively contribute to the concept  $h_y^{(t)}$ .

## 4. Experiments

We evaluate CAVE against existing concept-based approaches in terms of classification performance, robustness

to OOD data, and benchmark metrics on interpretability. For comparison, we consider the state-of-the-art post-hoc concept discovery approaches CRAFT [36], MCD [37], ICE [42], and PCX [9]. We further consider Label-Free CBMs [29], and the prototype learning approaches ProtoP-Net [7], TesNet [39], and PIP-Net [26], which all are inherently interpretable. Further details are given in A. 10.

## 4.1. Evaluation Metrics for Interpretability

**Benchmark Metrics.** For our evaluation, we consider the quality properties of the Co-12 explanation [27]. Our metrics are designed to quantify key properties that address the question: *to what extent are our explanations aligned with human-annotated object parts?* This includes:

1. **Part IoU and Local Coverage**
  - (i) *Part IoU* measures the overlap between the concept mask and the ground-truth object part, ignoring relevance of individual pixels. Thus, a concept with high overlap but minimal class relevance can still achieve a high score.
  - (ii) *Local Coverage* addresses the limitations of the previous metrics by weighting IoU with relevances, ensuring both overlap and contribution are considered.
2. **Global Coverage** evaluates how well detected concepts cover (i) the union of all ground truth object parts and (ii) the entire ground truth object. If coverage is high, the explanation remains stable and generalisable across different object views, even under occlusion.
3. **Entropy-based Pureness** measures how *concentrated* a concept is within a single object part. A highly pure concept is assigned mainly to one specific object part, rather than being distributed across multiple parts.

Formal definitions of these metrics are provided in A. 9.

**3D Consistency of Concepts.** A learned concept for an object should consistently map to the same region in the object. In particular, if the object is correctly learned, it should be 3D consistent regarding pose and spatial orientation (e.g.

	<i>IoU</i> $\uparrow$	<i>Loc. Cov.</i> $\uparrow$	<i>Global Cov.</i> $\uparrow$ $\cup$ Parts	<i>Pure.</i> $\downarrow$	<i>3D-C.</i> $\downarrow$
CRAFT [36]	0.065	0.104	0.266	0.412	0.483
MCD-SSC [37]	<b>0.149</b>	<b>0.231</b>	<b>0.334</b>	0.647	0.725
ICE [42]	0.115	0.182	0.246	0.363	0.983
PCX [9]	0.081	0.135	0.301	0.575	0.555
LF CBM [29]	0.117	0.187	0.330	0.632	0.622
ProtoPNet [7]	0.108	0.177	0.240	0.526	0.680
TesNet [39]	0.120	0.192	0.242	0.592	0.694
PIP-Net R [26]	0.062	0.113	0.216	0.734	<b>0.330</b>
PIP-Net C [26]	0.076	0.146	0.205	<b>0.771</b>	<b>0.425</b>
CAVE (Ours)	<b>0.152</b>	<b>0.259</b>	<b>0.376</b>	<b>0.838</b>	0.636
					<b>1.053</b>

Table 2. **Interpretability evaluation** on Pascal-Part with benchmark metrics *IoU*, *Local Coverage*, *Global Coverage* and *Pureness* for concept-based explanation methods. 3D-Consistency (3D-C) is evaluated on Pascal3D+. All methods are evaluated using a ResNet-50 backbone. We test PIP-Net with both ResNet-50 (R) and ConvNext (C), as ConvNext is recommended.

front versus back wheel). Thus, we introduce an additional metric that we term *3D Consistency*, measuring how consistent a concept is mapped to a ground truth 3D model. Here, we use the available and correctly oriented CAD models of objects in Pascal3D+ [40], mapping the attributions of one concept to the faces of the CAD model. Our score is the difference of attributions accumulated in the faces between samples with *lower being better* – if in one sample the concept is attributed to a different region of the 3D model than in another sample, the difference between attributions per face will be large. For a detailed explanation and formal definition of the score, we refer to A. 9.

## 4.2. CAVE has interpretable & consistent concepts

Considering the above evaluation protocol, we use Pascal-Part to quantitatively assess whether CAVE recovers interpretable concepts regarding standard benchmark metrics from the field and provide the results in Tab. 2. Overall, we see that among existing inherently interpretable methods no approach consistently outperforms the others. Among post-hoc approaches, the recent MCD approach performs strongly in most metrics. CAVE outperforms all competitors, both post-hoc as well as inherently interpretable, across different metrics, ranking first on all but average Pureness. For pureness, however, we are evaluating matching with the annotated parts, rather than whether what the model learned is sensible; if the model learned the concept wheel, but rim and tire are annotated, it will receive a worse score because despite learning a meaningful concept. Hence, this metric has to be taken with a grain of salt. This is also reflected by the other scores: CAVE is best in learning concepts that meaningfully cover annotated parts (IoU), cover most of the parts and the object (Coverage metrics), and are consistently localised.

Inspecting concept attributed to image regions, we can observe this effect also qualitatively (see Fig. 6), where

Dataset	P3D+	Occluded P3D+			OOD-CV	P-Part
		0	[20, 40]	[40, 60]		
CRAFT [36]	93.5	81.3	62.6	37.8	66.2	73.0
MCD-SSC [37]	96.8	87.2	67.3	40.2	72.9	72.6
ICE [42]	97.0	85.5	64.5	39.9	74.0	73.4
PCX [9]	96.4	85.5	65.3	38.0	75.9	74.8
LF CBM [29]	<b>98.4</b>	89.5	68.7	40.9	<b>83.6</b>	<b>79.2</b>
ProtoPNet [7]	96.3	80.7	55.5	27.2	66.9	68.1
TesNet [39]	97.6	85.0	63.7	34.0	75.0	74.7
PIP-Net R [26]	96.1	88.3	<b>73.9</b>	<b>50.1</b>	63.1	67.1
PIP-Net C [26]	98.1	<b>90.7</b>	73.5	44.0	72.8	72.1
CAVE (Ours)	<b>99.4</b>	<b>96.9</b>	<b>86.6</b>	<b>54.7</b>	<b>81.4</b>	<b>87.4</b>

Table 3. **Classification accuracy** ( $\uparrow$ ) on Pascal3D+ (P3D+), Occluded Pascal3D+ with different levels of occlusions in %, OOD-CV with 5 nuisance factors (pose, shape, context, texture, and weather), and Pascal-Part (P-Part).

similar, semantically meaningful concepts are highlighted across images and across different target classes.

While only roughly approximated through a cuboid, the learned features still consistently map to meaningful regions on the ground truth 3D model provided with the data, even for such a sparse and complex structure as a bicycle (cf. Fig. 5).

## 4.3. CAVE is robust to OOD data

One particular goal of CAVE was to be *both*, robust and interpretable. To evaluate robustness, we consider the Pascal3D+ dataset with 3 levels of occlusion (Occluded P3D+), and OOD factors such as pose, shape, context, texture, and weather (OOD-CV dataset). We measure the performance in terms of accuracy and report the results in Tab. 3. To no surprise, all methods perform relatively well on standard Pascal3D+, with CRAFT being the worst when using the reconstructed features for the model output. CAVE performs best, with an almost ideal 99.4% accuracy. When introducing small levels of occlusion, covering 20 – 40% of the image, CAVE experiences only a slight deterioration in performance, other methods drop by about 10% in accuracy points. This trend continues for higher levels of occlusion, with CAVE outperforming all competitors, including LF-CBMs, by a margin. Also visually, CAVE shows to only use actual (non-occluded) object parts for classification (cf. Fig. 12). On OOD-CV, LF-CBM performs best (83.6% acc) with CAVE a close second (81.4% acc), while other methods achieve significantly worse performance. Taken together, CAVE provides a unique combination of inherent interpretability and robustness to OOD data that is unmatched by existing work.

## 5. Discussion

With CAVE, we presented a robust and inherently interpretable model for image classification and provide an at-



Figure 6. **Example concepts learned by CAVE.** We show qualitative visualisations of concepts learned for each class  $y \in \{\text{Motorcycle}, \text{Bus}, \text{Bottle}, \text{Car}, \text{Chair}, \text{Train}\}$ . For each, we show the concept attributed to the ground truth 3D CAD model (left) showing spatially consistent concept learning, and visualise attributions in example images from different angles (right).



Figure 7. **Qualitative visualisations of concepts learned for class Car (top) and Boat (bottom).** Note that the same colors are used for both classes, but the concepts they represent are distinct between Car and Boat.

tribution method able to retrieve actually relevant input features for model decisions. Through extensive experiments with available part annotations, we found that CAVE finds the most consistent and interpretable concepts among a wide range of concept discovery and extraction methods, while being robust to OOD data.

As with all evaluations of interpretability, our evaluation is dependent on available benchmark datasets with ground truth annotation. While this annotation might not be the ideal, we here cover different aspects of interpretability through a diverse set of benchmark metrics established in the literature, and a new measure of 3D consistency, to provide a fair ground for evaluation.

One limitation specific to CAVE, as well as the original NOVUM [20], is the need for annotated poses during training. Yet, through this additional annotation we not only drastically increase robustness, but also get more consistent and interpretable features compare to standard 2D models by learning 3D object representations. Moreover, off-the-shelf object pose estimation methods [34] allow to annotate datasets for training of CAVE in down-stream applications.

A further potential limitation is the use of cuboids as 3D object representations, which allow to learn object representations flexibly and efficiently, but might poorly approximate the true shape of an object. In our experiments, however, we found that the concepts learned on cuboids project to meaningful and well-localised object regions even for sparse and complex 3D objects (cf. Fig. 5, 6).

## 6. Conclusion

We introduced CAVE, a robust and inherently interpretable image classifier that learns concept-aware neural object volumes. Through these volumes, our approach avoids Plato’s dilemma of the prisoners in the cave, learning meaningful 3D object representations instead of only representing a flattened 2D world like a shadow on the wall. We showed that the discovered concepts on these 3D representations are spatially consistent and better aligned with human-annotated object parts, all while robustly performing in classification across various OOD settings.

## References

- [1] David Alvarez Melis and Tommi Jaakkola. Towards robust interpretability with self-explaining neural networks. *Advances in neural information processing systems*, 31, 2018. [2](#)
- [2] Marco Ancona, Enea Ceolini, Cengiz Öztïreli, and Markus Gross. Towards better understanding of gradient-based attribution methods for deep neural networks. In *International Conference on Learning Representations*, 2018. [2](#)
- [3] Christopher J. Anders, David Neumann, Wojciech Samek, Klaus-Robert Müller, and Sebastian Lapuschkin. Software for dataset-wide xai: From local explanations to global insights with Zennit, CoRelAy, and ViRelAy. *CoRR*, abs/2106.13200, 2021. [5](#)
- [4] Sebastian Bach, Alexander Binder, Grégoire Montavon, Frederick Klaušen, Klaus-Robert Müller, and Wojciech Samek. On pixel-wise explanations for non-linear classifier decisions by layer-wise relevance propagation. *PloS one*, 10(7):e0130140, 2015. [3, 5](#)
- [5] Moritz Böhle, Mario Fritz, and Bernt Schiele. B-cos networks: Alignment is all we need for interpretability. In *IEEE/CVF Conference on Computer Vision and Pattern Recognition (CVPR)*, 2022. [2](#)
- [6] Chun-Hao Chang, Elliot Creager, Anna Goldenberg, and David Duvenaud. Explaining image classifiers by counterfactual generation. In *International Conference on Learning Representations*, 2019. [2](#)
- [7] Chaofan Chen, Oscar Li, Daniel Tao, Alina Barnett, Cynthia Rudin, and Jonathan K Su. This looks like that: deep learning for interpretable image recognition. *Advances in neural information processing systems*, 32, 2019. [2, 3, 6, 7, 4, 5](#)
- [8] Xianjie Chen, Roozbeh Mottaghi, Xiaobai Liu, Sanja Fidler, Raquel Urtasun, and Alan Yuille. Detect what you can: Detecting and representing objects using holistic models and body parts. In *Proceedings of the IEEE conference on computer vision and pattern recognition*, pages 1971–1978, 2014. [3, 4](#)
- [9] Maximilian Dreyer, Reduan Achtibat, Wojciech Samek, and Sebastian Lapuschkin. Understanding the (extra-) ordinary: Validating deep model decisions with prototypical concept-based explanations. In *Proceedings of the IEEE/CVF Conference on Computer Vision and Pattern Recognition*, pages 3491–3501, 2024. [2, 6, 7, 4, 5](#)
- [10] Gabriel Erion, Joseph D Janizek, Pascal Sturmels, Scott M Lundberg, and Su-In Lee. Improving performance of deep learning models with axiomatic attribution priors and expected gradients. *Nature machine intelligence*, 3(7):620–631, 2021. [2](#)
- [11] Thomas Fel, Mélanie Ducoffe, David Vigouroux, Rémi Cadène, Mikael Capelle, Claire Nicodème, and Thomas Serre. Don’t lie to me! robust and efficient explainability with verified perturbation analysis. In *Proceedings of the IEEE/CVF Conference on Computer Vision and Pattern Recognition*, pages 16153–16163, 2023. [2](#)
- [12] Thomas Fel, Victor Boutin, Louis Béthune, Rémi Cadène, Mazda Moayeri, Léo Andéol, Mathieu Chalvidal, and Thomas Serre. A holistic approach to unifying automatic concept extraction and concept importance estimation. *Advances in Neural Information Processing Systems*, 36, 2024. [2, 4, 1](#)
- [13] Jonas Fischer, Anna Olah, and Jilles Vreeken. What’s in the box? exploring the inner life of neural networks with robust rules. In *International Conference on Machine Learning*, pages 3352–3362. PMLR, 2021. [2](#)
- [14] Ruth C Fong and Andrea Vedaldi. Interpretable explanations of black boxes by meaningful perturbation. In *Proceedings of the IEEE International Conference on Computer Vision*, pages 3429–3437, 2017. [2](#)
- [15] Stephanie Fu, Mark Hamilton, Laura E. Brandt, Axel Feldmann, Zhoutong Zhang, and William T. Freeman. Featup: A model-agnostic framework for features at any resolution. In *The Twelfth International Conference on Learning Representations*, 2024. [2](#)
- [16] Amirata Ghorbani, James Wexler, James Y Zou, and Been Kim. Towards automatic concept-based explanations. *Advances in Neural Information Processing Systems*, 32, 2019. [3](#)
- [17] Sheng He, Yanfang Feng, P Ellen Grant, and Yangming Ou. Segmentation ability map: Interpret deep features for medical image segmentation. *Medical image analysis*, 84:102726, 2023. [2](#)
- [18] Robin Hesse, Simone Schaub-Meyer, and Stefan Roth. Fast axiomatic attribution for neural networks. *Advances in Neural Information Processing Systems*, 34:19513–19524, 2021. [2](#)
- [19] Ji Hou, Saining Xie, Benjamin Graham, Angela Dai, and Matthias Nießner. Pri3d: Can 3d priors help 2d representation learning? In *Proceedings of the IEEE/CVF International Conference on Computer Vision*, pages 5693–5702, 2021. [2](#)
- [20] Artur Jesslen, Guofeng Zhang, Angtian Wang, Wufei Ma, Alan Yuille, and Adam Kortylewski. Novum: Neural object volumes for robust object classification. In *European Conference on Computer Vision*, pages 264–281. Springer, 2024. [2, 3, 8, 1](#)
- [21] Pang Wei Koh, Thao Nguyen, Yew Siang Tang, Stephen Mussmann, Emma Pierson, Been Kim, and Percy Liang. Concept bottleneck models. In *International Conference on Machine Learning*, pages 5338–5348. PMLR, 2020. [2](#)
- [22] Maximilian Xiling Li, Korbinian Franz Rudolf, Nils Blank, and Rudolf Lioutikov. An overview of prototype formulations for interpretable deep learning. 2025. [3](#)
- [23] Julien Mairal, Francis Bach, Jean Ponce, et al. Sparse modeling for image and vision processing. *Foundations and Trends® in Computer Graphics and Vision*, 8(2-3):85–283, 2014. [4](#)
- [24] Alireza Makhzani and Brendan Frey. K-sparse autoencoders. *Proceedings of the International Conference on Learning Representations (ICLR)*, 2014. [3](#)
- [25] Meike Nauta, Ron Van Bree, and Christin Seifert. Neural prototype trees for interpretable fine-grained image recognition. In *Proceedings of the IEEE/CVF conference on computer vision and pattern recognition*, pages 14933–14943, 2021. [2](#)

- [26] Meike Nauta, Jörg Schlötterer, Maurice Van Keulen, and Christin Seifert. Pip-net: Patch-based intuitive prototypes for interpretable image classification. In *Proceedings of the IEEE/CVF Conference on Computer Vision and Pattern Recognition*, pages 2744–2753, 2023. 2, 3, 6, 7, 4
- [27] Meike Nauta, Jan Trienes, Shreyasi Pathak, Elisa Nguyen, Michelle Peters, Yasmin Schmitt, Jörg Schlötterer, Maurice Van Keulen, and Christin Seifert. From anecdotal evidence to quantitative evaluation methods: A systematic review on evaluating explainable ai. *ACM Computing Surveys*, 55(13s):1–42, 2023. 6
- [28] Fahimeh Hosseini Noohdani, Parsa Hosseini, Aryan Yazdan Parast, Hamidreza Yaghoubi Araghi, and Mahdieh Soleymani Baghshah. Decompose-and-compose: A compositional approach to mitigating spurious correlation. In *Proceedings of the IEEE/CVF Conference on Computer Vision and Pattern Recognition*, pages 27662–27671, 2024. 1
- [29] Tuomas Oikarinen, Subhro Das, Lam M Nguyen, and Tsui-Wei Weng. Label-free concept bottleneck models. In *The Eleventh International Conference on Learning Representations*, 2023. 2, 3, 6, 7, 4, 5
- [30] Seitaro Otsuki, Tsumugi Iida, Félix Doublet, Tsubasa Hirakawa, Takayoshi Yamashita, Hironobu Fujiyoshi, and Komei Sugiura. Layer-wise relevance propagation with conservation property for resnet. In *European Conference on Computer Vision*, pages 349–364. Springer, 2024. 3, 5, 6
- [31] Karl Schulz, Leon Sixt, Federico Tombari, and Tim Landgraf. Restricting the flow: Information bottlenecks for attribution. *arXiv preprint arXiv:2001.00396*, 2020. 2
- [32] Daniel Smilkov, Nikhil Thorat, Been Kim, Fernanda Viégas, and Martin Wattenberg. Smoothgrad: removing noise by adding noise. *arXiv preprint arXiv:1706.03825*, 2017. 3
- [33] Jost Tobias Springenberg, Alexey Dosovitskiy, Thomas Brox, and Martin A. Riedmiller. Striving for simplicity: The all convolutional net. In *International Conference on Learning Representations, Workshop Track Proceedings*, 2015. 3
- [34] Jiaming Sun, Zihao Wang, Siyu Zhang, Xingyi He, Hongcheng Zhao, Guofeng Zhang, and Xiaowei Zhou. OnePose: One-shot object pose estimation without CAD models. *CVPR*, 2022. 8
- [35] Mukund Sundararajan, Ankur Taly, and Qiqi Yan. Axiomatic attribution for deep networks. In *International Conference on Machine Learning*, pages 3319–3328. PMLR, 2017. 3
- [36] Fel Thomas, Picard Agustin, Bethune Louis, Boissin Thibaut, Vigouroux David, Colin Julien, Cadène Rémi, and Serre Thomas. Craft: Concept recursive activation factorization for explainability. In *Proceedings of the IEEE Conference on Computer Vision and Pattern Recognition (CVPR)*, 2023. 2, 6, 7, 4
- [37] Johanna Vielhaben, Stefan Blücher, and Nils Strodthoff. Multi-dimensional concept discovery (mcd): A unifying framework with completeness guarantees. *Trans. Mach. Learn. Res.*, 2023, 2023. 2, 6, 7, 4
- [38] Angtian Wang, Yihong Sun, Adam Kortylewski, and Alan L Yuille. Robust object detection under occlusion with context-aware compositionalnets. In *Proceedings of the IEEE/CVF Conference on Computer Vision and Pattern Recognition*, pages 12645–12654, 2020. 3, 4
- [39] Jiaqi Wang, Huafeng Liu, Xinyue Wang, and Liping Jing. Interpretable image recognition by constructing transparent embedding space. In *Proceedings of the IEEE/CVF International Conference on Computer Vision*, pages 895–904, 2021. 3, 6, 7, 4
- [40] Yu Xiang, Roozbeh Mottaghi, and Silvio Savarese. Beyond pascal: A benchmark for 3d object detection in the wild. In *IEEE winter conference on applications of computer vision*, pages 75–82. IEEE, 2014. 3, 7, 4
- [41] Yuanwen Yue, Anurag Das, Francis Engelmann, Siyu Tang, and Jan Eric Lenssen. Improving 2d feature representations by 3d-aware fine-tuning. In *European Conference on Computer Vision*, pages 57–74. Springer, 2024. 2
- [42] Ruihan Zhang, Prashan Madumal, Tim Miller, Krista A Ehinger, and Benjamin IP Rubinstein. Invertible concept-based explanations for cnn models with non-negative concept activation vectors. In *Proceedings of the AAAI Conference on Artificial Intelligence*, pages 11682–11690, 2021. 2, 6, 7, 4
- [43] Bingchen Zhao, Shaozuo Yu, Wufei Ma, Mingxin Yu, Shenxiao Mei, Angtian Wang, Ju He, Alan Yuille, and Adam Kortylewski. Ood-cv: A benchmark for robustness to out-of-distribution shifts of individual nuisances in natural images. In *European conference on computer vision*, pages 163–180. Springer, 2022. 3, 4

# Escaping Plato’s Cave: Robust Conceptual Reasoning through Interpretable 3D Neural Object Volumes

## Supplementary Material

### 7. Comparing Concept Spaces: Neural Volumes vs. Feature Activations

An advantage of an image classifier with neural object volumes is that it enhances the separation of the representation space, ensuring that Gaussian features from different classes remain well-distinguished [20]. Naturally, this is also the case for activations of features within the same classifier (cf. Fig. 8), which then leads us to examine where concept extraction is most effective. Our CAVE framework extracts class-wise concepts directly from neural object volumes  $\mathcal{G}$ , whereas traditional methods rely on activations from training features. We explore whether  $\mathcal{G}$  provides a more meaningful concept space by following three key steps:

1. extracting concepts using low-rank approximations (e.g., NMF). For a fair comparison, we use NMF as our extraction method because it is known to effectively extract meaningful and interpretable concepts from activations [12]. Note that NMF is not guaranteed to be the optimal choice for neural volumes  $\mathcal{G}$ .
2. projecting activations into the concept space, and
3. train a K-means clustering model on training image activations and evaluate it on test activations across different occlusion levels for concept separation.

A well-structured concept space should produce well-separated and compact clusters, which can be evaluated using the Silhouette Score and Davies-Bouldin Index (DBI). The Silhouette Score ranges from  $[-1, 1]$ , where 1 indicates optimal separation and values near 0 suggest overlapping clusters. In contrast, the Davies-Bouldin Index measures the ratio of intra-cluster dispersion to inter-cluster separation, with lower values indicating better-separated, more compact clusters. We also show 2D low-dimensional representations comparing the concept spaces of neural volumes and training activations across different classes in Fig. 9.

Occlusion	0	[20, 40]	[40, 60]	[60, 80]
NOVs $\mathcal{G}$	<b>0.343</b>	<b>0.333</b>	<b>0.335</b>	<b>0.338</b>
Activations	0.034	0.040	0.037	0.033

Table 4. Silhouette scores ( $\uparrow$ ) averaged across all classes in Pascal3D+, comparing concept spaces derived from neural object volumes  $\mathcal{G}$  and traditional activations. Higher scores indicate more compact clusters, with values close to 1 representing well-structured concept spaces. Results are reported across different occlusion levels in %.

Occlusion	0	[20, 40]	[40, 60]	[60, 80]
NOVs $\mathcal{G}$	<b>1.154</b>	<b>1.155</b>	<b>1.162</b>	<b>1.137</b>
Activations	2.365	2.348	2.306	2.318

Table 5. Davies-Bouldin Index ( $\downarrow$ ) averaged across all classes in Pascal3D+, comparing concept spaces derived from neural object volumes  $\mathcal{G}$  and traditional activations. Lower score means better cluster separation.

### 8. Details on Concept Extraction in CAVE

#### Ablation on Concept Extraction Methods

To choose the best concept extraction method on the object volumes for our CAVE model, we evaluate the extracted concept representations based on three metrics: accuracy, sparsity and FDD. We choose K-Means on the observation that its trade-off on accuracy is marginal, while its interpretability and faithfulness reflected in sparsity and FDD respectively are the best. We further visualise the trade-off between cluster quality, which is measured in within-cluster sum of squares ( $\downarrow$ ) for K-means, cumulative explained variance ( $\uparrow$ ) for PCA, and reconstruction error ( $\downarrow$ ) for NMF, versus number of clusters (cf. Fig. 10).

	Accuracy (%), $\uparrow$	Sparsity ( $\uparrow$ )	FDD ( $\downarrow$ )
K-Means	99.36	<b>0.95</b>	<b>0.32</b>
PCA	<b>99.39</b>	0.00	0.39
NMF	99.25	0.63	0.83
NOVUM	99.5	-	-

Table 6. The concept extraction methods are applied on the neural volumes  $\mathcal{G}_j \in \mathcal{G}$  in image classifier NOVUM with  $d = 20$  concepts. Each result is averaged across all classes from the Pascal3D+ dataset.

#### Attribute Relevance in Concept Extraction Methods

Note that how we compute concept attributions differs slightly depending on the concept extraction method.

- *K-Means*: Since each Gaussian feature is *hard-assigned* to a concept, the concept attribution is simply the sum of the relevance scores for all assigned Gaussians.
- *PCA & NMF*: These methods use *soft assignments*, meaning each Gaussian contributes to multiple concepts. Here, the concept attributions are weighted by their respective soft assignment values.

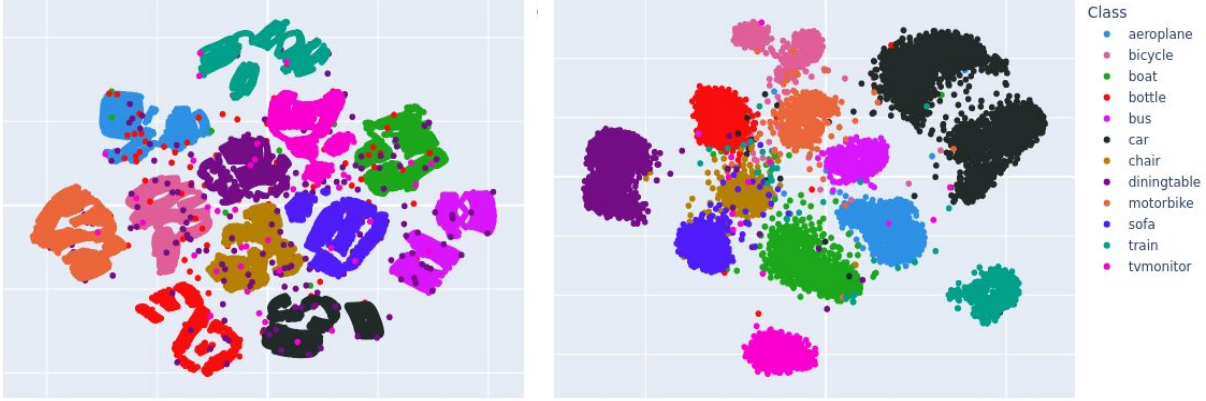


Figure 8. **Representation spaces** derived from neural object volumes  $\mathcal{G}$  (left) and activations of features (right).

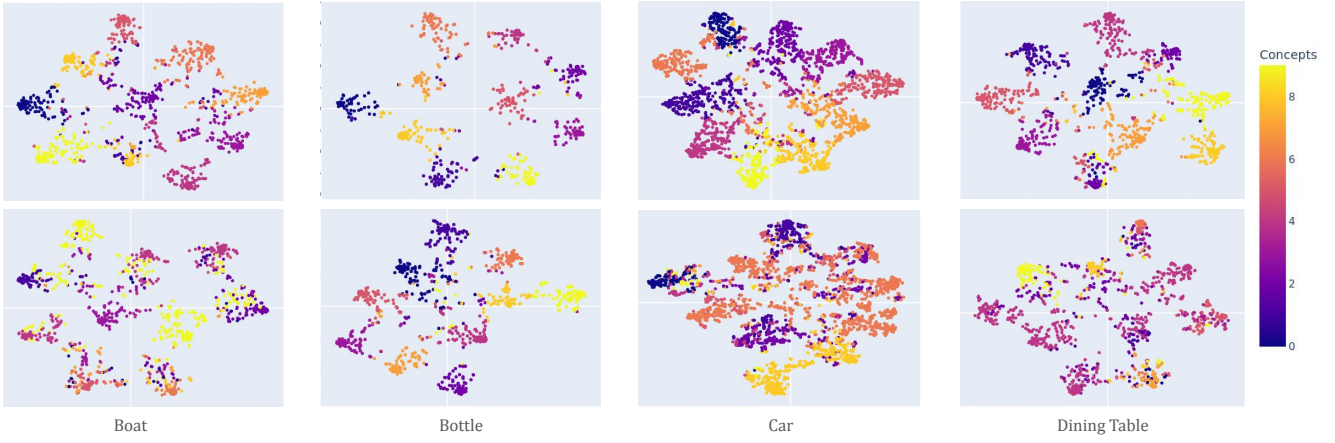


Figure 9. **t-SNE projection of concept embeddings in neural volume space (top) vs. activation space (bottom) for four classes in Pascal3D+.** Concepts in neural volume space are more well-separated and compact compared to those extracted from activation space.

## 9. Interpretability Metrics

### Part IoU and Local Coverage

The goal of these two metrics is to measure how well a concept *localises* in a ground-truth object part. Previous work including [14, 31] measures how well the attribution map  $A_m$  of a concept  $c_m$  aligns with a specific, interpretable part of an object that are defined as the ground truth region  $b_k$ . Specifically, it calculates the proportion of positive attributions that fall within  $b_k$ . However, this approach has a limitation: if a concept attributions  $A_m$  is concentrated within  $b_k$  but only covers a small portion of it, it may still yield a high score despite not comprehensively representing the object part.

On another hand, Intersection over Union (IoU) has been used widely in object detection, which can also be applied within this context to measure how well a concept covers  $b_k$  [6]. In specific, given an input image  $x$ , IoU is defined as:

$$IoU_{m,k}(x) = \frac{\sum_{i,j} (\mathbb{1}_m(i,j) \cdot \mathbb{1}_k(i,j))}{\sum_{i,j} \mathbb{1}_{m,k}(i,j)}, \quad (1)$$

where  $\mathbb{1}_m(i,j)$ ,  $\mathbb{1}_k(i,j)$ , and  $\mathbb{1}_{m,k}(i,j)$  are binary indicators for the concept region, ground-truth region and union of both regions respectively. Subsequently, IoU does not differentiate between pixels with varying attribution strengths, treating all contributing pixels equally.

Therefore, in addition to IoU, our evaluation includes Local Coverage to weight IoU with relevances, defined similarly to Dice-Sørensen coefficient that has been used also in XAI evaluation [17]:

$$LC_{m,k}(x) = \frac{\sum_{i,j} A_m^+(i,j) \cdot \mathbb{1}_k(i,j) + \mathbb{1}_m(i,j) \cdot \mathbb{1}_k(i,j)}{\sum_{i,j} A_m^+(i,j) + \sum_{i,j} \mathbb{1}_k(i,j)}, \quad (2)$$

where  $A_m^+(i,j)$  is the positive attribution given at pixel  $(i,j)$ . Local coverage score  $LC_{m,k}(x) \in [0, 1]$ . A concept

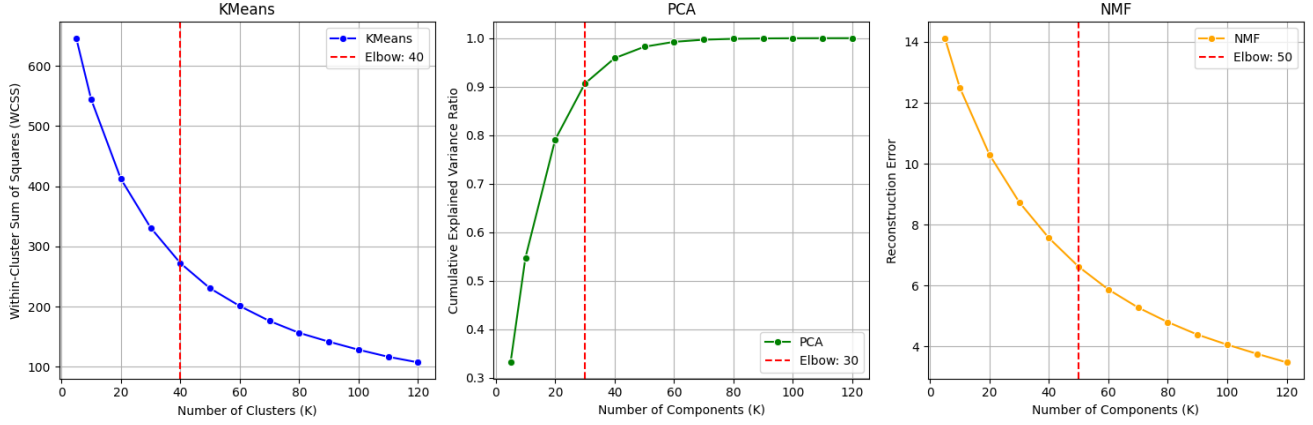


Figure 10. **Ablation on number number of concepts.** We show how well the different approaches to identify latent structure perform in terms of the corresponding metric of data structure recovery (y-axis) for varying latent dimension respectively cluster number (x-axis).

$c_m$  with a good local coverage not only has high relevances in ground-truth region  $b_k$  but also covers it well.

### Global Coverage

Understanding how well detected concepts *encompass* the ground-truth object is crucial. In the case of occlusion, a well-covered set of concepts enhances robustness, as it can still identify other visible, unoccluded parts. To do so, we first normalise the attributions so that the total attribution across all concepts for a given input sums to 1. This means that if all the concepts perfectly collide with ground-truth part mask, the coverage score is 1. This also ensures a fair and consistent comparison between different methods.

$$\tilde{A}_m^+(i, j) = \frac{A_c^+(i, j)}{\sum_{m'} \sum_{i,j} A_{m'}^+(i, j)}. \quad (3)$$

The global coverage metric can be computed with respect to either the union of all ground-truth object parts or the object bounding box. The advantage of the former is that it provides a more precise evaluation by focusing only on meaningful object regions, avoiding background noise. However, given that such annotation is often incomplete, we also include the latter for a more comprehensive evaluation. For an input image  $x$ , we define the

$$GC_{\cup\text{Parts}}(x) = \sum_{i,j} \sum_m \tilde{A}_m^+(i, j) \cdot \min \left( 1, \sum_k \mathbb{1}_k(i, j) \right), \quad (4)$$

which denotes the total positive attributions that also contributes to the ground-truth masks. The term  $\min(1, \sum_k \mathbb{1}_k(i, j))$  ensures that the overlapping masks are treated as a single region. Similarly, we also define the formula for object bounding box:

$$GC_{\text{Object}}(x) = \sum_{i,j} \sum_m \tilde{A}_m^+(i, j) \cdot \mathbb{1}_{\text{bbox}}(i, j). \quad (5)$$

Naturally,  $GC(x) \in [0, 1]$  for both cases, with a higher score means better coverage.

### Pureness

This evaluation metric focuses on how distinct a detected concept  $c$  with respect to ground-truth part annotation  $b_k$  [26]. A concept is considered *pure* if its attributions are concentrated within a single meaningful object part  $b_k$  rather than being distributed across multiple parts. Formally, pureness of a concept  $c_m$  is defined as follows:

$$P_m(x) = - \sum_k O_{m,k} \log O_{m,k}. \quad (6)$$

with

$$O_{m,k} = \frac{\sum_{i,j} A_m^+(i, j) \cdot \mathbb{1}_k(i, j)}{\sum_{i,j} A_c^+(i, j)}.$$

A lower score indicates better purity.

### 3D Consistency

A desired property of concept is meaningfulness [16], and a concept must be consistent to be meaningful. Ensuring consistency of spatial location of a latent concept is thus crucial. To this end, we propose a metric for 3D Consistency that evaluates how well a concept maintains its *spatial integrity* across different object viewpoints. Formally, given an input image  $x$  of class  $y$ , using known camera parameters, we project each pixel in  $A_m^+(i, j)$  onto the corresponding faces  $\Omega_y$  of the given CAD model (in correct orientation) of class  $y$ . For a class concept  $c_m$ , the score is then computed across a set of  $N$  images of class  $y$ , denoted  $\mathcal{X}$ , as follows:

$$C_{3D}(\mathcal{X}, c_m) = \frac{1}{N^2} \sum_{x \neq x' \in \mathcal{X}} \|\Omega_y(A_m^+(x)) - \Omega_y(A_m^+(x'))\|_1, \quad (7)$$

Classes	# Images	# Valid Images
0. Aeroplane	643	554
1. Bicycle	418	342
2. Boat	388	321
3. Bottle	341	272
4. Bus	347	285
5. Car	687	616
6. Chair	490	302
7. Dining Table	173	154
8. Motorbike	372	319
9. Sofa	346	276
10. Train	407	341
11. TV Monitor	384	323
<b>Total</b>	<b>4996</b>	<b>4186</b>

Table 7. Number of evaluation samples per class in the Pascal-Part dataset. Grayed-out classes do not have meaningful part annotations.

Dataset	Accuracy (%), ↑						
	P3D+	Occluded P3D+	[20, 40]	[40, 60]	[60, 80]	OOD-CV	P-Part
Occlusion	0	[20, 40]	[40, 60]	[60, 80]	-	-	0
ResNet-50	98.1	92.5	78.9	51.2	73.4	77.5	
NOVUM	99.5	97.2	88.6	59.2	82.8	88.7	

Table 8. Accuracy of ResNet-50 and NOVUM on Pascal3D+ (P3D+), Occluded-P3D+ and OOD-CV, and Pascal-Part (P-Part).

with  $C_{3D}(\mathcal{X}, c) \in [0, 2]$ . In essence, for each sample we accumulate attributions in the faces of the CAD model, and compare the differences in these vectors of face attributions between any pair of samples from the class  $y$ . Thus, a lower score means better consistency. We include the class-wise 3D consistency scores for all methods in Tab. 9. For a fair comparison, we exclude background concepts (e.g., present in less than 50% test images) since those will not be mapped to the object CAD model and the result distance will be always 0 across these concepts.

## 10. Experimental Setup and Optimisation

### Datasets

We evaluate the accuracy of our method CAVE and other baselines on multiple datasets: Pascal3D+ [40], Occluded P3D+ [38] with three levels of occlusion [20, 40], [40, 60] and [60, 80]%, OOD-CV [43] and Pascal-Part [8]. All methods, except for post-hoc approaches, are trained on Pascal3D+ training split and evaluated on these aforementioned datasets. For OOD-CV dataset, since two classes Bottle and TV Monitor are not present, we exclude their logit scores when computing predictions. For Pascal-Part, we filter the dataset to include only the 12 object classes

present in Pascal3D+ and cross-reference them to identify test images that also appear in Pascal3D+ (cf Tab. 7). For quantitative interpretability metric, we use Pascal-Part dataset where ground-truth part annotation is available. Four classes Boat, Chair, Dining Table, and Sofa do not have part annotations.

During training for baselines, the images are resized to  $224 \times 224$  resolution. We normalise pixel values using the ImageNet mean and standard deviation. For CAVE, the images are resized to  $640 \times 800$ , with object-centric view.

### Architecture

All methods have ResNet-50 backbone, except for PIP-Net where we also include ConvNext backbone as it is recommended. Our CAVE leverages the backbone of NOVUM, which also has ResNet-50 as its feature extractor. We provide ResNet-50 and NOVUM performance across our evaluation datasets in Tab. 8.

### Implementation Details

We follow the implementation provided by the original authors [7, 9, 26, 29, 36, 37, 39, 42] for our baselines:

1. For post-hoc methods including CRAFT, ICE, and PCX, we used the exact setting provided in their codebases, except for the number of class-wise concepts being 20. For MCD-SSC, we use completeness threshold of 0.7 instead of default 0.5 to discover a meaningful number of concepts.
2. For Label Free CBM, we followed the codebase instructions to generate a concept set, resulting in 441 concepts. We then trained a ResNet-50v2 label-free CBM using their hyperparameters: learning rate 0.1, batch size 512, CLIP model ViT-B/16, and interpretability cutoff 0.45. Unlike post-hoc approaches, where the number of concepts is fixed at 20, label-free CBM learns this number dynamically. After training, we observed 297 non-zero weights out of 5292, yielding roughly 5% sparsity.
3. For ProtoPNet and TesNet, we used the exact training hyperparameters from their codebases: the prototype activation function is log, with regular add-on layers, a training batch size of 80, and a training push batch size of 75. The learning rates for features, add-on layers, and prototype vectors are set to  $1e-4$ ,  $3e-3$ ,  $3e-3$  respectively, with a joint learning rate step size of 5. The projection (push) step was performed every 10 epochs. The network was trained for 100 epochs without a warm-up period and without extensive data augmentation to ensure fairness across all baselines.
4. For PIP-Net, we trained the network using the hyperparameter settings from its codebase. Specifically, during pre-training, we used a batch size of 128 and trained for 10 epochs. For the main training phase, we used a batch size of 64 and trained for 60 epochs. The learning rate was set to 0.05 with no weight decay.

Methods	Aeroplane	Bicycle	Boat	Bottle	Bus	Car	Chair	Dining Table	Motorbike	Sofa	Train	TV Monitor	<b>Mean</b>
CRAFT	1.388	1.304	1.303	1.207	1.398	1.472	1.367	1.192	1.305	1.320	1.304	1.063	1.302
MCD-SSC	1.609	1.706	1.622	1.330	1.645	1.667	1.498	1.227	1.705	1.500	1.578	1.009	1.508
ICE	1.542	1.570	1.558	0.934	1.340	1.486	1.195	0.900	1.536	1.049	1.354	0.578	1.253
PCX	1.305	1.079	1.718	1.416	1.440	1.735	1.028	1.228	—	—	1.522	0.750	1.322
Label-free CBM	1.576	1.617	1.580	1.225	1.552	1.669	1.533	1.293	1.681	1.490	1.563	1.085	1.489
ProtoPNet	1.636	1.616	1.665	1.351	1.636	1.509	1.485	1.219	1.632	1.550	1.630	0.952	1.490
TesNet	1.678	1.639	1.532	1.284	1.605	1.680	1.466	1.211	1.640	1.450	1.563	0.913	1.472
PIP-Net R	1.345	1.484	1.280	1.347	1.741	1.041	1.330	1.097	1.646	1.412	1.383	0.876	1.332
PIP-Net C	1.532	1.616	1.413	1.407	1.740	1.362	1.453	1.357	1.687	1.558	1.476	1.031	1.469
<b>CAVE (Ours)</b>	1.190	1.434	1.159	0.632	1.043	1.230	1.169	0.991	1.344	0.958	0.906	0.575	<b>1.053</b>

Table 9. **Class-wise 3D Consistency Scores on Pascal3D+** averaged across all concepts for each class, with L1 distance.



Figure 11. **Example of a car with 40% occlusion**, where methods like LCBM [29], PCX [9], and ProtoPNet [7] fail to provide reliable explanations due to their sensitivity to missing object parts. Unlike the other methods, CAVE (**Ours**) focuses on more informative regions despite the occlusion, demonstrating better resilience to missing object parts. This highlights the importance of *robust explanations* when dealing with real-world challenges.



Figure 12. **Layer-wise relevance was propagated in CAVE from the output prediction to the pixel space under four different occlusion levels:** no occlusions, [20, 40], [40, 60], and [60, 80]. In all cases, CAVE accurately highlights the unoccluded parts of the object, demonstrating its robustness in handling occlusions and ensuring reliable explanations even under challenging conditions.

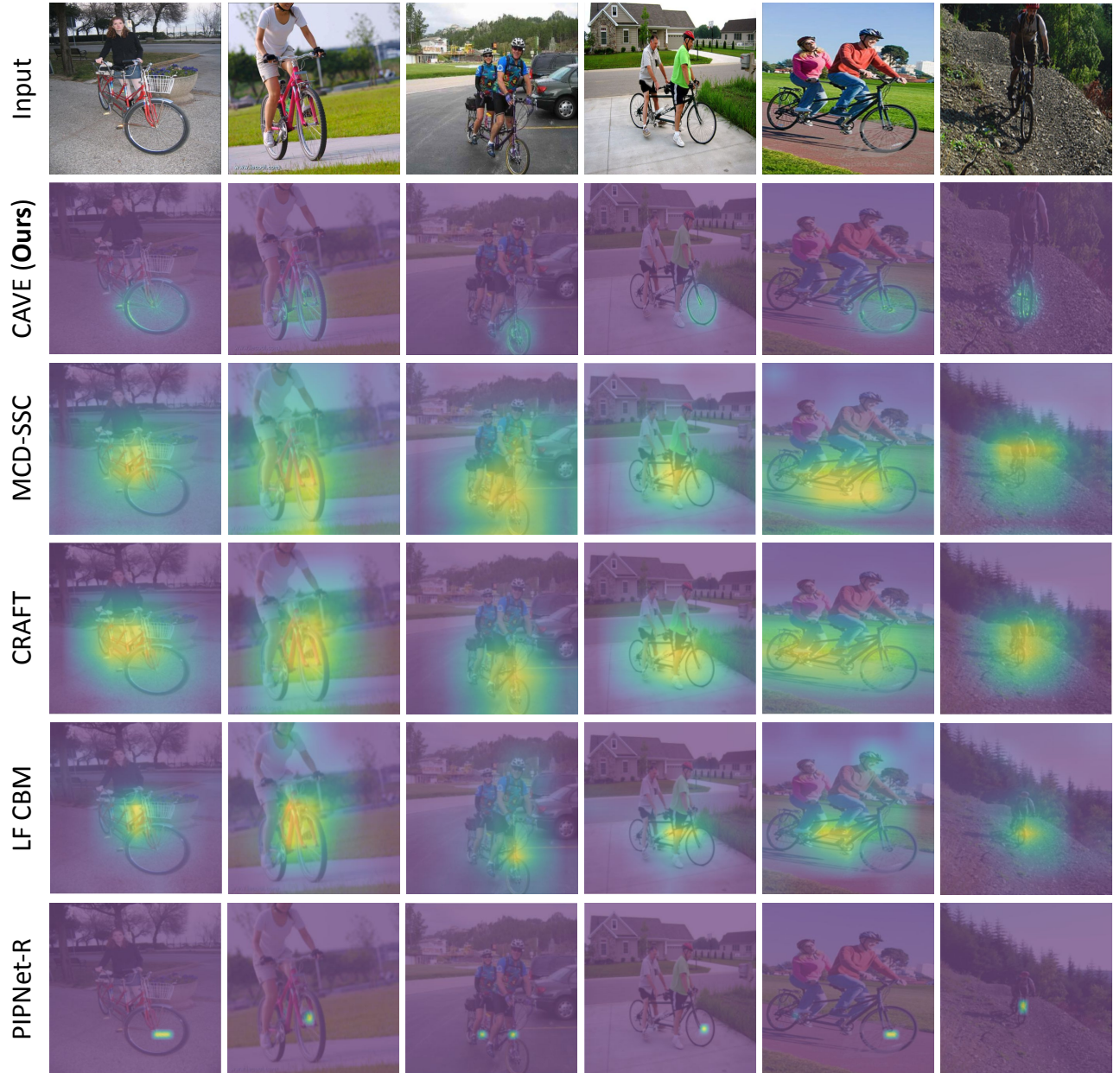
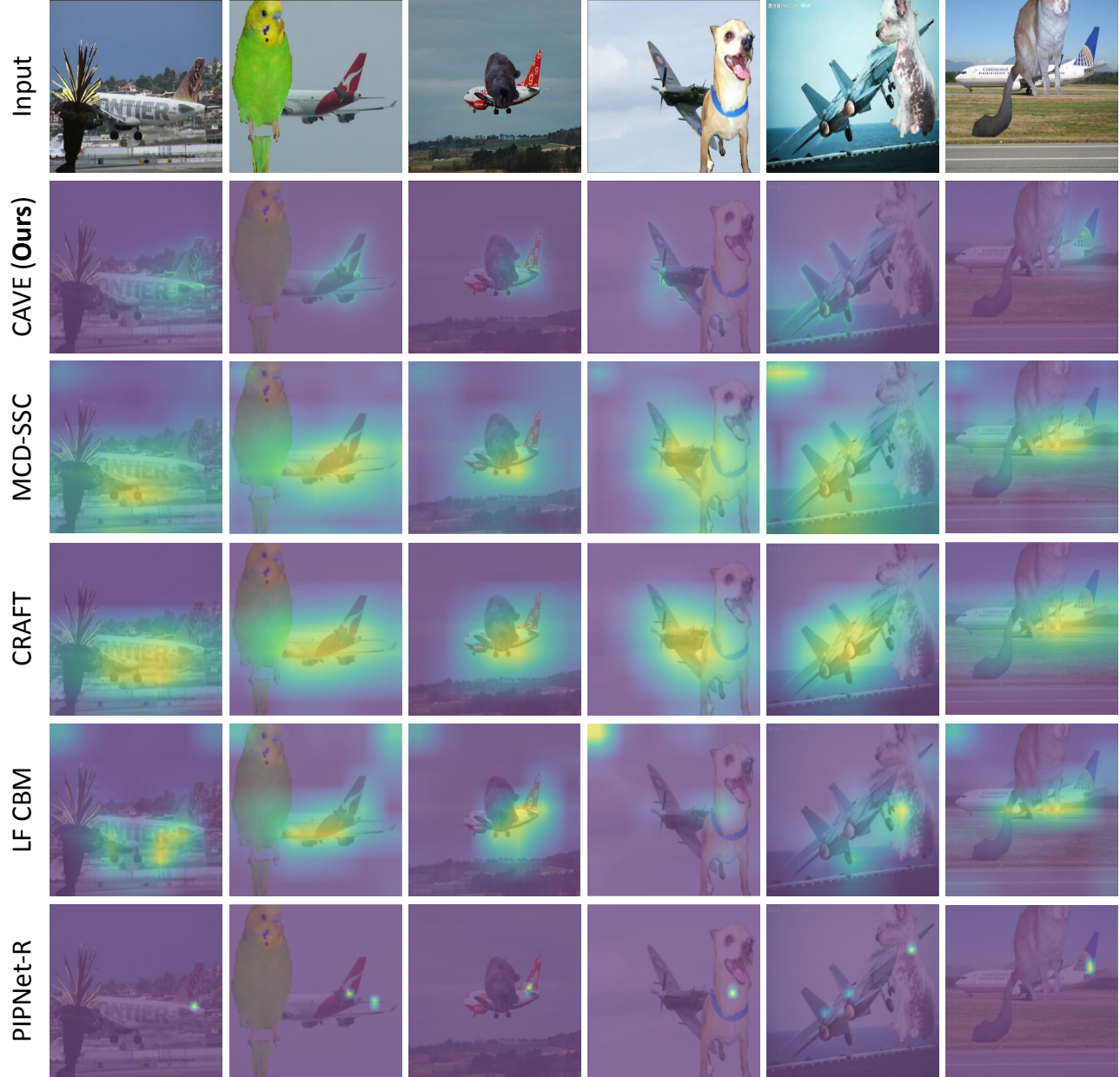


Figure 13. Qualitative examples of concepts detected by CAVE (Ours) vs. a selection of baseline methods MCD, CRAFT, LF CBM and PIPNet-R for class Bicycle with no occlusion. Our explanations consistently highlight concept that seems to be *front wheel*, whereas for baseline methods such as MCD-SSC, CRAFT, and LF CBM, the concepts are mixing between *wheels*, *bike frame*, and *human*.



**Figure 14. Qualitative examples of concepts detected by CAVE (Ours) vs. a selection of baseline methods MCD, CRAFT , LF CBM and PIPNet-R for class Aeroplane with occlusion level 20 – 40%. Our explanations consistently highlight concept that seems to be vertical & horizontal stabilisers and refrain from occluded object parts. Whereas for baseline methods, the explanations appear inconsistent and partially highlight image regions where the object parts are not visible.**

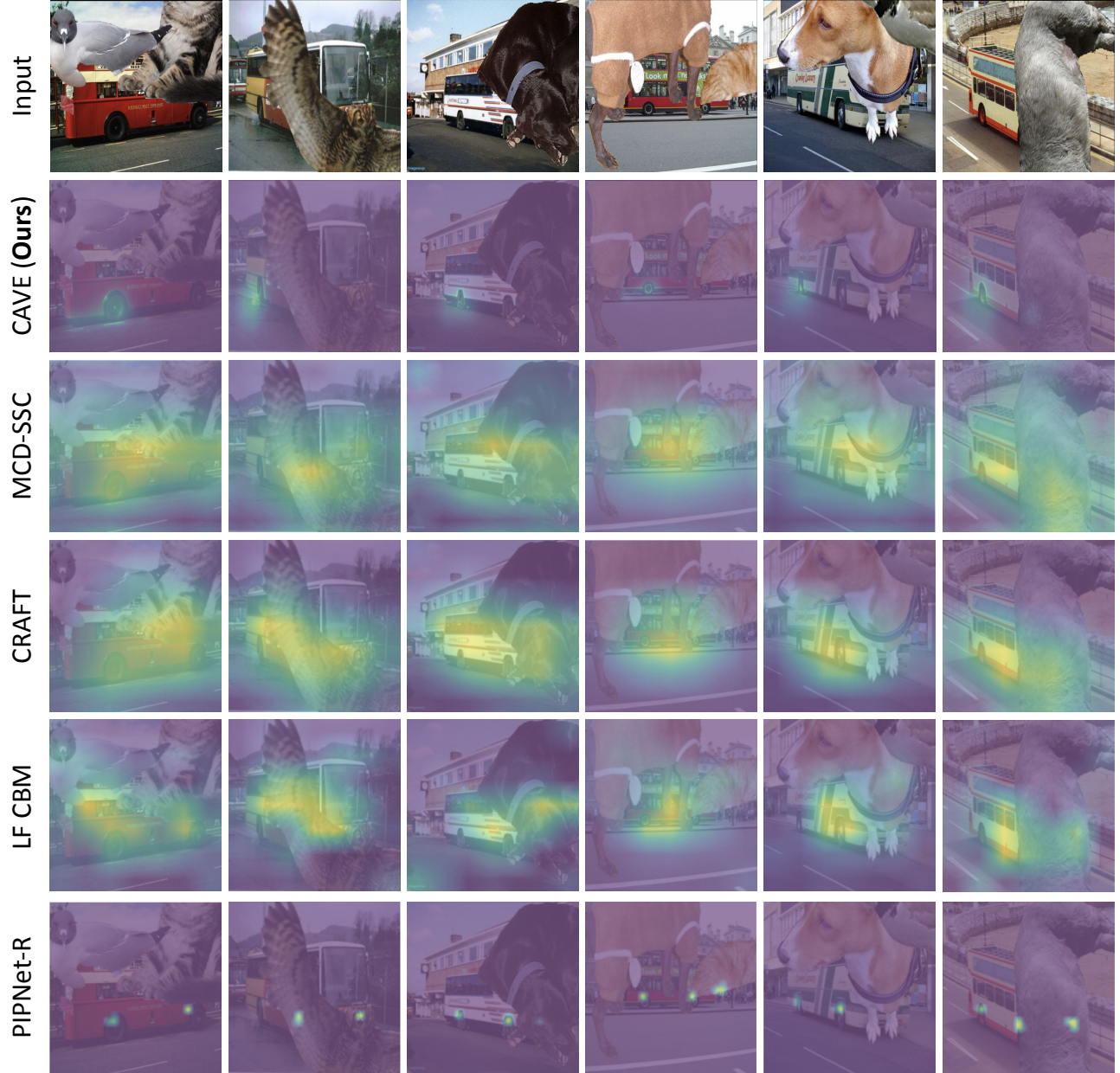
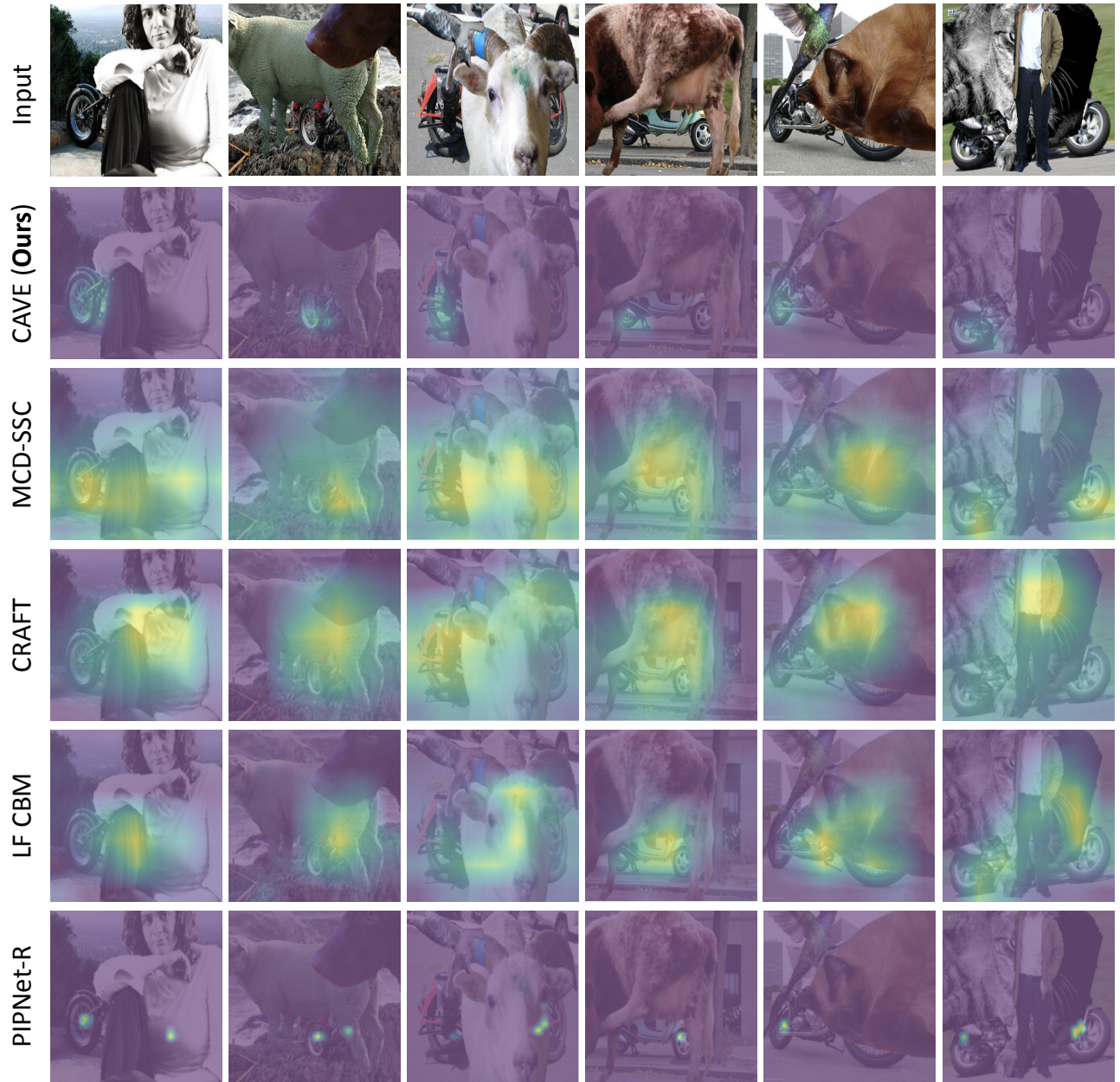


Figure 15. Qualitative examples of concepts detected by CAVE (Ours) vs. a selection of baseline methods MCD, CRAFT , LF CBM and PIPNet-R for class Bus with occlusion level 40 – 60%. Our explanations consistently highlight concept that seems to be *rear wheel* and refrain from occluded object parts. Whereas for baseline methods, the explanations appear inconsistent and partially highlight image regions where the object parts are not visible.



**Figure 16. Qualitative examples of concepts detected by CAVE (Ours) vs. a selection of baseline methods MCD, CRAFT , LF CBM and PIPNet-R for class Motorcycle with occlusion level 60 – 80%.**  Our explanations consistently highlight concept that seems to be *wheel* and refrain from occluded object parts. Whereas for baseline methods, the explanations appear inconsistent and partially highlight image regions where the object parts are not visible.